Direct-Current Triboelectric Generator

*Ya Yang, Hulin Zhang, and Zhong Lin Wang**

The first direct-current triboelectric generator (DC-TEG) based on sliding electrification for harvesting mechanical energy from rotational motion is reported. The DC-TEG consists of two rotating wheels and one belt for connecting them, which are made of distinctly different triboelectric materials with a specific requirement. During the rotation, the contact-induced electrification and the relative sliding between the two wheels and the belt can induce a continuous increase of the accumulated positive and negative triboelectric charges at the two rotating wheels, respectively, resulting in a Corona discharge and producing the observed current through an external load. The DC-TEG can deliver an open-circuit voltage of larger than 3200 V and a maximum power of 100 μW under an external load of 60 MΩ at a rotational speed of 1000 r min^{-1}. By designing a point metal discharge electrode near the accumulated positive charges on the metal wheel, the instantaneous short-circuit current can be up to 0.37 mA. The DC-TEG can be utilized as a direct power source to light up 1020 serially connected commercial light-emitting diodes (LEDs) and the produced energy can also be stored in a capacitor for other uses. This work presents a DC-TEG technology to harvest mechanical energy from rotational motion for self-powered electronics.

1. Introduction

Harvesting ambient mechanical energy has attracted increasing attention in the past decade for not only enabling the self-powered electronic devices/systems, but also meeting the rapid-growing worldwide energy consumptions.[1–3] Renewable mechanical energy harvesting techniques based on electrostatic, electromagnetic, and piezoelectric effects have been developed to charge batteries for portable electronics and sensor systems.[4–6] Recently, we have demonstrated an innovative approach to harvest mechanical energy from impacts, sliding, and rotations by utilizing triboelectric generators (TEGs).[7–11] Owning to the coupling between triboelectrification and electrostatic induction, all of the reported TEGs exhibit an alternating-current (AC) output characteristics either in the periodic contact-separation mode or sliding mode,[12–17] resulting in that the produced triboelectric charges can not be continuously accumulated unless a rectification bridge circuit is used. One solution would be to develope the direct current (DC)-TEG technology to scavenge mechanical energy, leading to the flow of current in one direction and the continuous collection of the triboelectric charges for the some specific applications.

In this paper, we report the first DC-TEG including two rotatable wheels and one belt for connecting them, which are made of three different triboelectric materials with a specific design. During the rotation process, the contact-induced electrification and the relative sliding between the wheel and the belt can result in a continuous increase of the accumulated positive and negative triboelectric charges at the two rotating wheels, respectively. A Corona discharge results in the flow of electrons through an external load. The DC-TEG can deliver an open-circuit voltage of 3200 V and a maximum power of 100 μW under an external load of 60 MΩ, where the short-circuit current can be up to 0.37 mA by designing a point discharge electrode near the accumulated positive charges on the metal wheel. We also demonstrated that the DC-TEG can be used to directly light up 1020 LEDs and the produced energy can also be stored in a capacitor.

2. Results and Discussion

As schematically illustrated in **Figure 1**a, the design of the DC-TEG relies on three different triboelectric materials with a tribo-polarity of $\alpha_{III} > \alpha_{I} > \alpha_{II}$ according to the ability to lose electrons. The device is composed of two rotational wheels (II and III) and one belt (I) to connect them, where the wheel II is connected to a rotational motor. The electrode E_2 is near the wheel II and the electrode E_1 is contacted with the wheel III. The reference point T was used to monitor the relative sliding length of the belt. Figure 1b illustrates the charge distribution in the device when the belt passes the reference point T with a length of L_{AB}. According to the triboelectric series,[18] the electrons are injected from wheel III to belt I, resulting in positive and negative triboelectric charges on the wheel III and the belt (the section of L_{AB}) surfaces, respectively. The surface of the belt at the section of L_{DA} also has the negative triboelectric charges due to the separation between the wheel III and the belt at the section of L_{DA}. Moreover, since the wheel II is much more

Dr. Y. Yang, H. Zhang, Prof. Z. L. Wang
School of Materials Science and Engineering
Georgia Institute of Technology
Atlanta, GA 30332, USA
E-mail: zlwang@gatech.edu
Prof. Z. L. Wang
Beijing Institute of Nanoenergy and Nanosystems
Chinese Academy of Sciences
Beijing, China

DOI: 10.1002/adfm.201304295

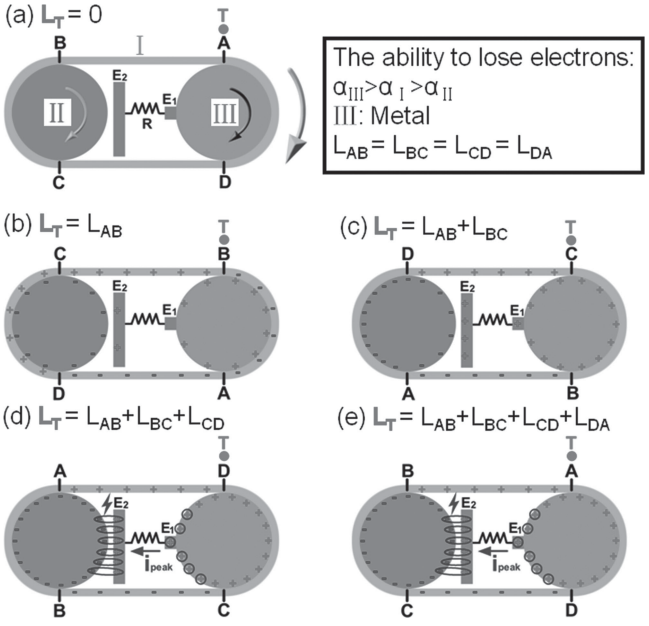

Figure 1. Working mechanism of the DC-TEG. a) Initial status without sliding motion of the belt. b–e) The triboelectric charge distributions when the belt I went through the point T with the length of L_{AB}, $L_{AB} + L_{BC}$, $L_{AB} + L_{BC} + L_{CD}$, and $L_{AB} + L_{BC} + L_{CD} + L_{DA}$, respectively. L_T is the length that the belt went through the reference point T. L_{AB} is the length of the belt between A and B.

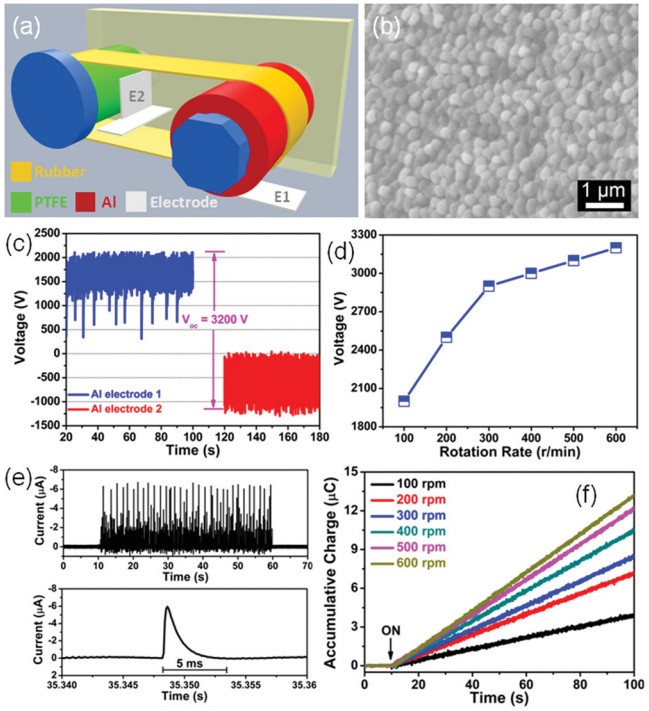

Figure 2. a) Schematic diagram of the DC-TEG. b) SEM image of the PTFE surface. c) The measured surface electrical potentials at the electrodes E_1 and E_2. d) Open-circuit voltage of the DC-TEG at different rotational speeds. e) Short-circuit current of the DC-TEG at a rotational speed of 100 r min^{-1}. f) Accumulative inductive charges generated by the DC-TEG at different rotational speeds.

triboelectrically negative than the belt I, a contact between the wheel II and the belt (the section of L_{CD}) can result in negative and positive charges on the contact surfaces, as shown in Figure 1b. Due to the separation between the wheel ? and the belt (the section of L_{CD}), the surface of the belt (the section of L_{CD}) has the positive triboelectric charges. With increasing the passed length of the belt at the reference point T, more and more negative and positive charges (Figure 1c,d) are accumulated at the wheel II and wheel III, respectively. Moreover, some positive charges were accumulated at the electrode E_2 due to the electrostatic induction. As displayed in Figure 1d, a discharge between the wheel II and the electrode E_2 occurs due to the high electric field induced electrical breakdown of air (e.g., Corona discharge), which can drive the flow of electrons from electrode E_2 to electrode E_1, producing a DC pulse signal in the external circuit. This discharge can periodically appear in the rotation process due to the periodical increase of the accumulated triboelectric charges, and there is a current if Corona discharge occurs, as shown in Figure 1e. Thus, the working principle of the fabricated device in this study is based on a continuously accumulated positive and negative triboelectric charges on the two wheels in the rotational process to induce an electrical breakdown of air (Corona discharge) to drive the flow of electrons in the external load.

The fabricated DC-TEG consists of a polytetrafluoroethylene (PTFE) wheel, an Al wheel and a rubber belt (the ability to lose electrons: $\alpha_{Al} > \alpha_{Rubber} > \alpha_{PTFE}$), as schematically illustrated in **Figure 2**a. Figure S1 (Supporting Information) presents the side view of a typical as-fabricated DC-TEG, where the rubber belt has a width of 2 cm. The distance between the PTFE wheel and the electrode E_2 is about 2 mm and the electrode E_1 is contacted with the Al wheel. To increase the negative triboelectric charge density, the PTFE nanoparticles were produced, as shown in Figure 2b. The diameters of the PTFE particles are smaller than 500 nm. The introduced nanostructure can be utilized to increase the surface roughness and the effective surface area of the triboelectric materials, which can induce a larger triboelectric charge density and improve the efficiency of triboelectrification. The surface nanostructure can be created via an inductively coupled plasma (ICP) method or by being functionalized using variety of molecules, composited with nanowires/nanotubes or nanoparticles for tuning the surface characteristics. Figure 2c shows the measured surface electric potentials of the electrodes E_1 and E_2 in the rotational process at a rotational speed of 600 r min^{-1}. The electrode E_1 has the positive surface electric potential of about 2100 V, which is associated with the accumulated positive triboelectric charges on the Al wheel. Moreover, the electrode E_2 has the negative surface electric potential of about –1100 V due to the accumulated negative triboelectric charges on the PTFE wheel. The obtained open-circuit voltage between the two electrodes is up to 3200 V. As displayed in Figure S2 (Supporting Information), the enlarged surface electric potential on the electrode E_2 shows a periodic discharge on the electrode, which can drive the flow of electrons between two electrodes. The open-circuit voltage of the device was found to increase with increasing the rotation speed, as shown in Figure 2d. Figure 2e presents that the measured short-circuit current of the DC-TEG is about 6 μA at a rotational speed of 100 r min^{-1}. The enlarged current-time

Adv. Funct. Mater. **2014**,
DOI: 10.1002/adfm.201304295

curve shows that the largest width of the output current peak is about 5 ms. As illustrated in Figure S3 (Supporting Information), the short-circuit current of the device can be larger than 15 μA at the rotational speed of about 1200 r min^{-1}, indicating that it can increase with increasing the rotational speed. However, when the electrode E_2 is in contact with the PTFE wheel, the short-circuit current decreases to about 5 μA, which is associated with the triboelectrification between the electrode E_2 and the PTFE wheel. Under forward connection, Figure 2f illustrates the accumulative charges at the different rotational speeds, indicating that the larger rotational speed can induce a larger charge quantity at the same time period. After reversely connecting the device to the measurement system, the obtained charge signal was also switched in sign, as displayed in Figure S4 (Supporting Information).

To confirm the DC output characteristic of the device, we measured the output voltage of the TEG when a loading resistance of 1 GΩ was connected between the two electrodes, as illustrated in **Figure 3**a. The output voltage of TEG is about 260 V under the forward and reversed connection conditions. The enlarged output voltage in Figure 3b clearly shows a DC voltage output signal. The output voltage of the device was found to decrease with decreasing the loading resistance, as displayed in Figure 3c. At the rotational speed of 1000 r min^{-1}, the short-circuit current of the device is about 13 μA and the enlarged current-time curve presents that the obtained current output signal has the DC characteristic, as illustrated in Figure 3d. Moreover, the output current of the device decreases with increasing the loading resistance, as depicted in Figure S5 (Supporting Information). Figure 3e shows the resistance dependence of both the output voltage and current with the resistance from 1 MΩ to 1 GΩ. The current drops with the increase of the loading resistance, while the output voltage of the device rises up with increasing the resistance. The maximum value of the output power is about 100 μW at a loading resistance of 60 MΩ, as illustrated in Figure 3f.

To demonstrate the ability of the device as a DC power source to power some electronics, a total of 65 commercial green LEDs were used as the external load. **Figure 4**a presents that these LEDs were divided into two groups, which were connected to the device with reversed polarity. The letters "TE" consist of 29 LEDs connected in series, while another 36 LEDs were connected in series with reversed polarity to produce the letters "NG". As illustrated in Figure 4b, the 29 LEDs with the letters "TE" were lighted up by the TEG in real time at a rotational speed of 1098 r min^{-1}, while no light emission can be observed from the other 36 LEDs with the letters "NG". It can be also seen in the Movie File-1 (see the Supporting Information). Moreover, when the connection direction between the TEG and the LEDs was reversed (Figure 4c), only the 36 LEDs with the letters "NG" can be lighted up, as displayed in Figure 4d. These results indicate that the fabricated TEG has the DC output characteristic, which is different from previous AC-TEG.[19] To illustrate that the device as an energy harvester for scavenging the rotation energy from tires, the DC-TEG was fabricated in the front wheel of a commercial bicycle, as depicted in Figure 4e. The enlarged photograph shows that the DC-TEG consists of a PTFE wheel, an Al wheel, and a rubber belt for connecting the two wheels. The DC-TEG was connected with 65 green LEDs in series, constituting the letters "TENG". Figure 4f displays that these LEDs can be lighted up when rotating the wheel of the bicycle, which can also be seen in the Movie File-2 (see the Supporting Information). These results indicate that the invented DC-TEG can be effectively utilized to scavenge the waste rotating mechanical energy.

To demonstrate that the DC-TEG can not only be used for lighting up tens of LEDs, but also for simultaneously driving a large

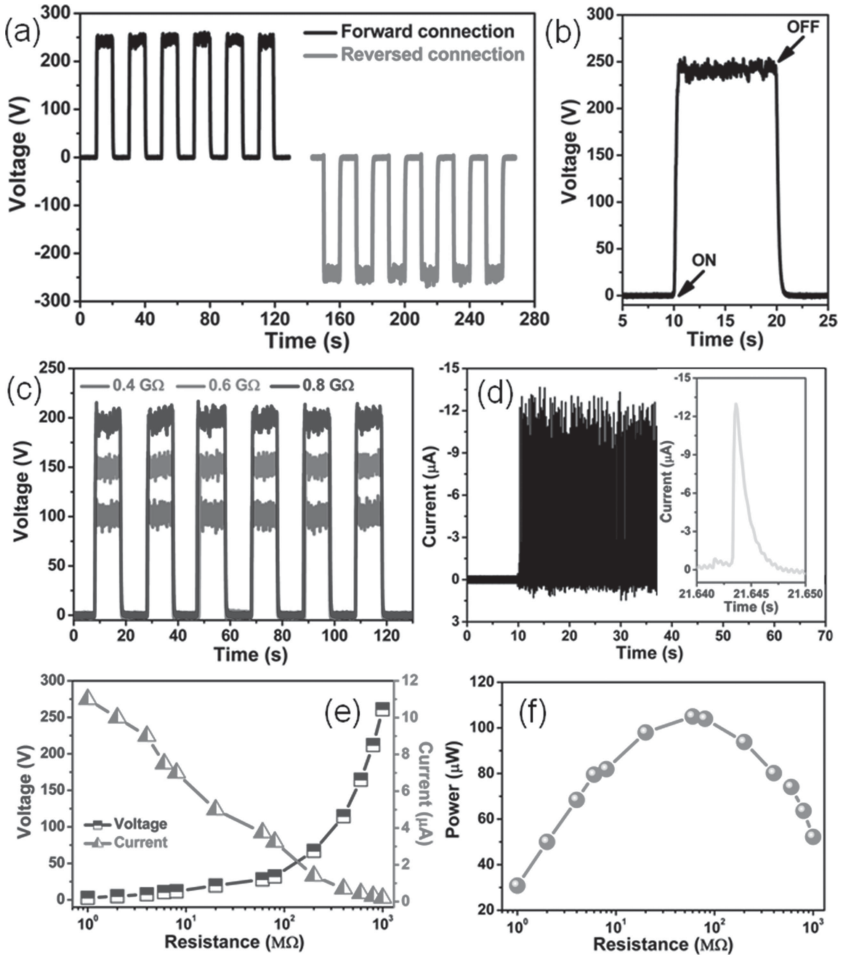

Figure 3. a) Output voltage of the DC-TEG under the forward and reversed connection conditions at the loading resistance of 1GΩ. b) Enlarged view of the output voltage-time curve. c) Measured output voltages under different loading resistances. d) Short-circuit current of the DC-TEG at a rotational speed of 1000 r min^{-1}. Inset: enlarged view of a single current peak. e,f) The dependence of e) the output voltage and current and f) the output power on the resistance of the external loading resistances.

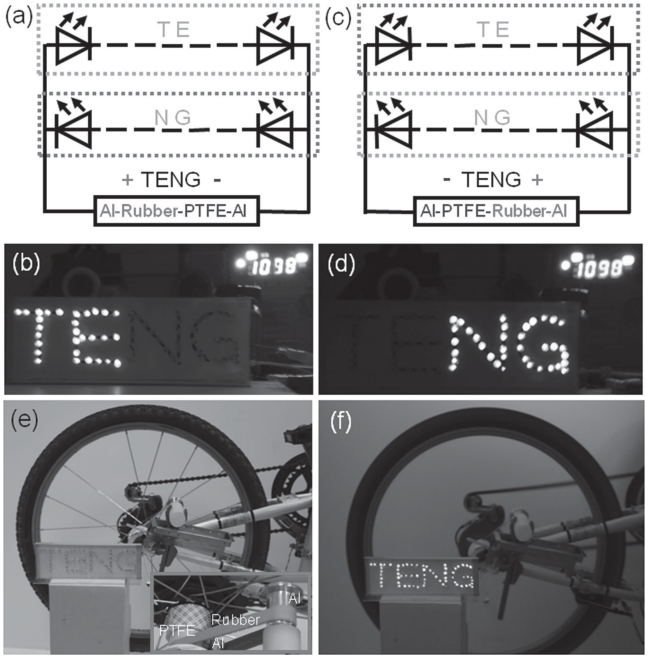

Figure 4. a) Schematic diagram of the connection between the DC-TEG and the green LEDs. b) Photograph of the DC-TEG driven LEDs with the letters "TE". c) Schematic diagram of the reversed connection between the DC-TEG and the green LEDs. d) Photograph of the LEDs with the letters "NG" lighted up by the DC-TEG. e) Photograph of the DC-TEG fabricated in a commercial bicycle. The inset shows the structures of the device. f) Photograph of the DC-TEG driven green LEDs with the letters "TENG".

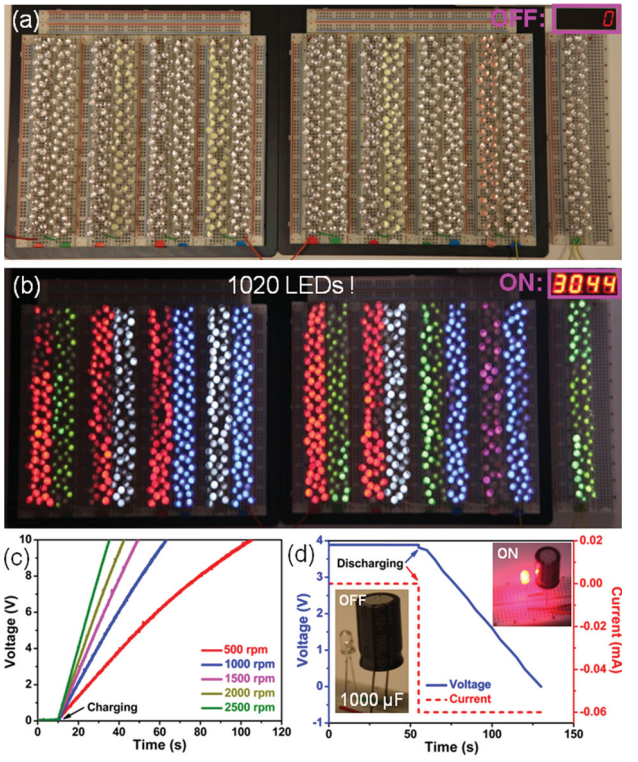

Figure 5. a,b) Photographs of the DC-TEG as a direct power source for driving 1020 LEDs when the DC-TEG is a) off and b) on at a rotational speed of 3044 r min^{-1}. c) The measured voltage of a 1 μF capacitor charged by the DC-TEG at the different rotational speeds. d) The constant-current discharging curves of a 1000 μF capacitor charged by the DC-TEG. The inset shows the photographs of the charged capacitor to light up a red LED.

number of electronic devices, 1020 commercial multicolor LEDs were connected in series to fabricate the LED panels, as depicted in **Figure 5**a. Under a rotational speed of 3044 r min^{-1}, the DC-TEG can be utilized to directly light up as many as 1020 LEDs, as illustrated in Figure 5b and the Movie File-3 (see the Supporting Information). Furthermore, the produced electric energy by the TEG can be also stored for further use. Figure 5c presents the charging curves of a capacitor (1 μF) by the DC-TEG under the different rotational speeds. The capacitor can be charged from 0 to 10 V within tens of seconds (95 s, 53 s, and 25 s at the rotational speeds of 500 r min^{-1}, 1000 r min^{-1}, and 2500 r min^{-1}, respectively), indicating that the efficiency of converting the mechanical energy to the stored electrical energy can be enhanced by increasing the rotational speed. Figure S6 (Supporting Information) displays that a capacitor of 1000 μF can be charged from 0 to 3.8 V in about 5 h at a rotational speed of 1000 r min^{-1}. Under a constant discharging current of 60 μA, the charged capacitor can last for about 74 s before it gets back to 0 V, corresponding to a total electric capacity of 1.3 μAh, as displayed in Figure 5d. The photographs (the inset in Figure 5d) show that the stored energy in the capacitor can be used to drive a red LED, as illustrated in the Movie File-4 (see the Supporting Information).

The fabricated DC-TEGs have a high open-circuit voltage of 3200 V but a low short-circuit current (<20 μA), as depicted in Figure 1, 2. To increase the output current of the DC-TEG, a single-electrode based DC-TEG was fabricated, as shown in Figure S7 (Supporting Information). The electrode E_2 is connected to ground, while the electrode E_1 is connected with a loading resistance and then to ground. In the rotational process, the electrons from ground were accumulated on the electrode E_1, and the holes were accumulated on the Al wheel. Due to the electrical breakdown of air between the electrode E_1 and the Al wheel, the discharge will result in the flow of electrons through the loading resistor from the ground to the electrode E_1. To enhance the discharge between the electrode E_1 and the Al wheel, an Al tip was designed as the electrode E_1, as illustrated in Figure S8 (Supporting Information). Under a loading resistance of 1 GΩ, the output voltage of the single-electrode based DC-TEG is about 240 V, as illustrated in **Figure 6**a. Moreover, the output voltage of the device decreases with decreasing the loading resistance, as displayed in Figure S9 (Supporting Information). As depicted in Figure 6b, the instantaneous short-circuit current can be up to 0.37 mA at the rotational speed of 1000 r min^{-1}, which is 20 times larger than that of the TEG in Figure 3. The enlarged current-time curve in Figure 6c shows that the largest width of the output current pulse is about 1 ms, which is smaller than that in Figure 2e. It indicates a faster discharge speed than that of the TEG in Figure 2e. The different output currents for the two kinds of DC-TEGs are associated with the different discharge materials. The discharge current between two metals is larger than that between an insulator material and a metal since the electrons can much more easily

DOI: 10.1002/adfm.201304295

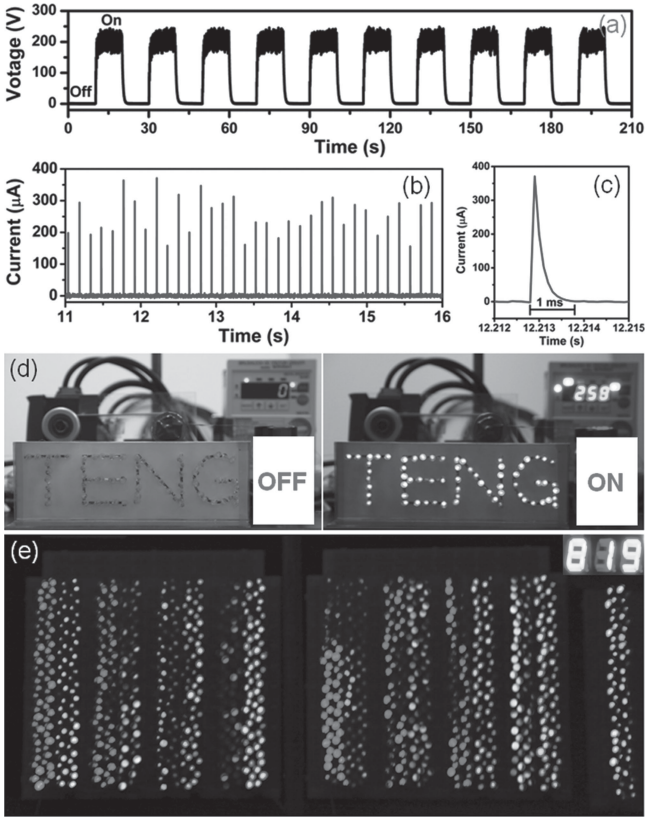

Figure 6. a) Output voltage of the single-electrode-based DC-TEG under a loading resistance of 1GΩ and at the rotational speed of 1000 r min^{-1}. b,c) Short-circuit current of b) the single-electrode-based DC-TEG and c) the enlarged view. d) Photographs of the green LEDs with the letters "TENG" when the DC-TEG is off and on. e) Photograph of the 1020 LEDs lighted up by the DC-TEG.

move in the metal than on the insulator surface.[20] The strong electrostatic discharges can result in the observed sparks, as shown in the Movie File-5 (see the Supporting Information). Figure S10 (Supporting Information) presents that the instantaneous output current of the TEG can be larger than 0.3 mA at the lower rotational speeds of 100 and 500 r min^{-1}, indicating that the TEG can be utilized to drive some electric devices at low rotational speeds. Figure 6d illustrates that the 65 commercial green LEDs can be driven by the DC-TEG at the rotational speed of 258 r min^{-1}, which can also be seen in the Movie File-6 (see the Supporting Information). Moreover, the 1020 LEDs can be lighted up at the rotational speed of 819 r min^{-1}, as displayed in Figure 6e and the Movie File-7 (see the Supporting Information). These results indicate that the DC-TEGs can harvest the mechanical energy from rotational motion at the low rotational speeds for self-sustained electronics.

It is necessary to compare the fabricated DC-TEG with the Van de Graaff generator (V_{dG}-G),[21] where the two devices are different in following aspects: 1) the different functions: the V_{dG}-G was designed for producing high voltage, while the DC-TEG has been designed for scavenging the mechanical energy to power some electronics; 2) the different device structures: the V_{dG}-G consists of the positive and negative spherical terminals and two transporting belts of silk or any other flexible insulating material, while DC-TEG is composed of two wheels and a belt with the three different triboelectric materials of a specific design; 3) the different working mechanisms: for the V_{dG}-G, an external voltage was usually used to spray the positive and negative charges to the transporting belts for transferring these charges to two metal spheres to induce a much higher voltage between the two spheres, which means that the current is from another source rather than self-generated; for the DC-TEG, no external power source is provided, and the contact-induced electrification and the relative sliding between the two wheels and the belt induce a continuos increase of the accumulated positive and negative triboelectric charges at the two rotating wheels, respectively, resulting in a Corona discharge for producing the observed current through an external load; 4) the different working conditions: The V_{dG}-G usually needs to connect with the ground or an external power source while the DC-TEG can work without connecting with the ground and the external power source. Moreover, as compared with the previous bridge curcuit equipped DC triboelectric generators, the invented DC-TEG has more advantages. The previous triboelectric generators can not be used to continually accumulate the charges; However, the invented DC-TEG in this study can be used to continually accumulate the charges, which can deliver the output voltage up to 3200 V for lighting up 1020 commercial LEDs and charging some electronic devices by harvesting the waste rotating mechanical energy.

3. Conclusions

In summary, we have demonstrated a DC-TEG, consisting of two rotatable wheels and one belt for connecting them, which are made of three different triboelectric materials with specific requirements. The mechanism of the DC-TEG is based on a continuously accumulated positive and negative triboelectric charges on the two wheels in the rotational process to induce an electrical breakdown of air (Corona discharge) to drive the flow of electrons in the external load. The fabricated TEG produces an open-circuit voltage of larger than 3200 V and a maximum power of 100 μW under an external load of 60 MΩ at a rotational speed of 1000 r min^{-1}, where the output performance can be further increased by applying a larger rotational velocity. The instantaneous short-circuit current of the TEG can be up to 0.37 mA by utilizing the discharge between a point metal electrode and the accumulated positive charges on the metal wheel. The DC-TEG can be used to directly light up 1020 serial-connected commercial LEDs and the produced energy can be also stored in a capacitor. This work may push forward a significant step toward the potential applications of the DC-TEG and the high voltage power source technologies.

4. Experimental Section

Fabrication of the DC-TEG: The DC-TEG consists of a PTFE wheel, an Al wheel and a rubber belt, where a PTFE film with the thickness of 1 mm was used to fabricate the PTFE wheel. Before etching process, we deposited a Au layer of about 20 nm on the PTFE as the mask.

The surface of the PTFE film can be dry-etched using ICP to create the nanoparticle structures, where the O_2, Ar, and CF_4 gases with flow ratio of 10, 15, and 30 sccm were introduced in the ICP chamber. Two power sources of 400 W and 100 W were used to generate a large density of plasma and accelerate the plasma ions, respectively. The PTFE film was etched for 60 s to produce the nanoparticle-like surface structures. The PTFE film was then fixed on a plastic wheel to produce the PTFE wheel. The two Al foils were used as the two electrodes E_1 and E_2, which are near the PTFE wheel (2 mm) and in contact with the Al wheel, respectively. For the DC-TEG in Figure 6, the electrode E_2 is connected with the ground and the loading resistor was connected between the electrode E_1 and the ground.

Measurement of the Fabricated DC-TEG: In the voltage and current measurement process, the TEGs were connected with a Keithley 6514 System Electrometer and a low-noise current preamplifier (Stanford Research SR570). The surface potential was measured by connecting the device electrode to an electrometer. The accumulative charges of the DC-TEG were measured by using the Keithley 6514 System Electrometer.

Supporting Information

Supporting Information is available from the Wiley Online Library or from the author.

Acknowledgements

This work was supported by Airforce, MURI, U.S. Department of Energy, Office of Basic Energy Sciences (DE-FG02–07ER46394), NSF, and the Knowledge Innovation Program of the Chinese Academy of Sciences (KJCX2-YW-M13). The authors thank Yuanjie Su, Xiandai Zhong, and Xiaonan Wen for their help in this work.

Received: December 27, 2013
Revised: January 24, 2014
Published online:

[1] Z. L. Wang, W. Wu, *Angew. Chem.* **2012**, *51*, 11700–11721.
[2] Z. L. Wang, *ACS Nano* **2013**, *7*, 9533–9557.
[3] Z. L. Wang, G. Zhu, Y. Yang, S. Wang, C. Pan, *Mater. Today* **2012**, *15*, 532–543.
[4] J. M. Donelan, Q. Li, V. Naing, J. A. Hoffer, D. J. Weber, A. D. Kuo, *Science* **2008**, *319*, 807–810.
[5] L. C. Rome, L. Flynn, E. M. Goldman, T. D. Yoo, *Science* **2005**, *309*, 1725–1728.
[6] P. D. Mitcheson, P. Miao, B. H. Stark, E. M. Yeatman, A. S. Holmes, T. C. Green, *Sens. Actuators, A* **2004**, *115*, 523–529.
[7] F.-R. Fan, Z.-Q. Tian, Z. L. Wang, *Nano Energy* **2012**, *1*, 328–334.
[8] S. Wang, L. Long, Z. L. Wang, *Nano Lett.* **2012**, *12*, 6339–6346.
[9] Y. Yang, H. Zhang, Z.-H. Lin, Y. S. Zhou, Q. Jing, Y. Su, J. Yang, J. Chen, C. Hu, Z. L. Wang, *ACS Nano* **2013**, *7*, 9213–9222.
[10] Y. Yang, H. Zhang, J. Chen, S. Lee, T.-C. Hou, Z. L. Wang, *Energy Environ. Sci.* **2013**, *6*, 1744–1749.
[11] L. Lin, S. Wang, Y. Xie, Q. Jing, S. Niu, Y. Hu, Z. L. Wang, *Nano Lett.* **2013**, *13*, 2916–2923.
[12] X.-S. Zhang, M.-D. Han, R.-X. Wang, F.-Y. Zhu, Z.-H. Li, W. Wang, H.-X. Zhang, *Nano Lett.* **2013**, *13*, 1168–1172.
[13] Y. Yang, H. Zhang, J. Chen, Q. Jing, Y. S. Zhou, X. Wen, Z. L. Wang, *ACS Nano* **2013**, *7*, 7342–7351.
[14] J. Zhong, Q. Zhong, F. Fan, Y. Zhang, S. Wang, B. Hu, Z. L. Wang, J. Zhou, *Nano Energy* **2013**, *2*, 491–497.
[15] Z. H. Lin, Y. Xie, Y. Yang, S. Wang, G. Zhu, Z. L. Wang, *ACS Nano* **2013**, *7*, 4554–4560.
[16] Y. Yang, L. Lin, Y. Zhang, Q. Jing, T.-C. Hou, Z. L. Wang, *ACS Nano* **2012**, *6*, 10378–10383.
[17] Y. S. Zhou, Y. Liu, G. Zhu, Z.-H. Lin, C. Pan, Q. Jing, Z. L. Wang, *Nano Lett.* **2013**, *13*, 2771–2776.
[18] L. S. McCarty, G. M. Whitesides, *Angew. Chem. Int. Ed.* **2008**, *47*, 2188–2207.
[19] P. Bai, G. Zhu, Y. Liu, J. Chen, Q. Jing, W. Yang, J. Ma, G. Zhang, Z. L. Wang, *ACS Nano* **2013**, *7*, 6361–6366.
[20] V. E. Shashoua, *J. Polym. Sci.* **1958**, *33*, 65–85.
[21] R. J. Van de Graaff, K. T. Compton, L. C. Van Atta, *Phys. Rev.* **1933**, *43*, 149–157.